


Two-step morphology-based denoising and non-local means smoothing improves micro-computed tomography digital rock images

Utkarsh Gupta¹ | Vijitha Periyasamy² | Ronny Hofmann³ | Jaya Prakash⁴ |
Phaneendra K. Yalavarthy¹ 

¹Department of Computational and Data Sciences, Indian Institute of Science, Bangalore, India

²Shell India Markets Private Ltd., Shell Technology Centre Bangalore, Mahadeva Kodigehalli, Bengaluru, India

³Shell International Exploration and Production Inc., Shell Technology Center Houston, Houston, Texas, USA

⁴Department of Instrumentation and Applied Physics, Indian Institute of Science, Bangalore, India

Correspondence

Phaneendra K. Yalavarthy, Department of Computational and Data Sciences, Indian Institute of Science, Bangalore 560 012, India. Email: yalavarthy@iisc.ac.in

Funding information

Shell India Markets Private Ltd.

Abstract

Digital rock physics is a workflow that relies on imaging techniques to quickly and cost-effectively estimate the petrophysical properties of small core samples taken from reservoirs. By using digital representations of rock samples as input, physics-based simulators can estimate properties such as porosity and permeability. The accuracy of these estimates depends on the quality of the digital volumes generated from micro-computed tomography scans. To enhance the accuracy, denoising is necessary to reduce image noise caused by various experimental factors like electronic noise and bad pixels. This study introduces a novel two-step denoising pipeline that combines adaptive morphological filtering with non-local means smoothing, ensuring both noise reduction and preservation of edges. The effectiveness of the proposed pipeline is assessed through qualitative evaluation using optimal segmentation results and quantitative evaluation using a non-reference metric and equivalent number of looks. Comparing the results of the two-step approach with traditional non-local means and morphology-based filtering using a multi-resolution structurally varying bitonic filter, the non-reference metric and equivalent number of looks values are higher, indicating improved denoising performance. Furthermore, the denoised rock volume is subjected to the next step in the digital rock workflow to compute important petrophysical properties like porosity and permeability. The findings indicate that our proposed pipeline significantly improves the accuracy of estimating physical parameters such as porosity and permeability.

KEYWORDS

computing aspects, data processing, imaging, noise, petrophysics, rock physics, tomography

INTRODUCTION

The digital rock (Al-Marzouqi, 2018; Andrä et al., 2013) workflow is an imaging-based workflow built on three-dimensional (3D) models of representative elementary rock volume, referred to as mini-core plugs drilled from the reservoir. A typical digital rock image analysis pipeline consists of acquiring micro x-ray computed tomography (μ -CT) projections of mini core plugs. These two-dimensional projections

obtained from different angles are used to reconstruct a 3D model of the rock sample (Gupta & Ranjan, 2022a, 2022b). These reconstructed models are further segmented, resulting in geometric models to identify solid and pore spaces in the rock. The geometric models are then used to perform numerical simulations of different physical phenomena like fluid flow, wave propagation, electric flow and other physical phenomena. Several petrophysical properties (i.e., porosity, permeability, etc.) can be estimated by these



physics-based simulations. Knowing these petrophysical properties is expected to reduce the cost and time invested in the special core analysis experiments which is the gold standard (Dvorkin et al., 2008). Accurate estimation of rock properties is crucial in determining the exploration investment in the reservoir, carbon capture and storage techniques and so on.

However, the quality of the 3D segmented rock models depends a lot on obtaining accurate μ -CT scans of the rock samples, which are often corrupted by large noise. Beam-hardening, partial volume effect, motion artefact, ring artefact, scattering, reconstruction approximations and so on are the shortcomings in the acquisition process that lead to the noise in the image (Sheppard et al., 2004; Wildenschild & Sheppard, 2013; S. Berg et al., 2018). Therefore, an appropriate pre-processing step that involves denoising of the μ -CT scans of rocks is mandatory. For rock image analysis, preserving the size of the narrowest corners and throats in the pore space is of primary importance; hence, it requires acquiring the scans at a high resolution. However, high-resolution scans are contaminated by more noise due to enormous scanning time and sampling theorem conditions (as high-resolution scans require estimation of high-frequency information). Thus a filtering step becomes a must when imaging at a high resolution. Typical segmentation algorithms are sensitive to the noise in the image, which further pushes the need for denoising algorithms designed for digital rock.

Different methodologies have been proposed in the literature to remove shot/Poisson noise (Verma & Ali, 2013; Zha & Qiu, 2006; Zha, 2007). Even though simple techniques like median filtering can be used for denoising, the denoised images result in a significant loss of resolution at the grain-pore boundary, which leads to inefficient segmentation at the pore-grain interface (Saxena et al., 2017). We specifically require a class of edge-preserving filters (Eibenberger et al., 2008) in the workflow since the pixels at the pore-grain boundary determine the flow of media (hydrogen, oil, water or mercury). Notably the narrow pore throats are of the utmost importance for accurate estimation of physical properties; hence, designing appropriate edge-preserving filters is crucial. Filters like anisotropic diffusion (Sheppard et al., 2004) and bilateral filter (Verri et al., 2017) have been a default choice in the workflow in the past as they preserved significant features while denoising. From recent literature on digital rock (Saxena et al., 2019; Andr a et al., 2013; Verri et al., 2017; Sell et al., 2016; Sun et al., 2017; Dong et al., 2020; Reshetova et al., 2020), we observe a switch to non-local means (NLM) filtering (Buades et al., 2005) as it has proven to be more adaptive and efficient in preserving edges while denoising (S. Berg et al., 2018). Hence, we have considered NLM filtering as the base filter technique to compare our proposed denoising pipeline. The NLM algorithm is a patch-based technique and tries to denoise based on similar patches in the imaging domain. However, these methods are

based on pixel-based smoothing and tend to provide blurry denoised image.

Recently, deep learning (DL) techniques have been used in the digital rock workflow at almost every level to enhance the performance of the workflow. DL techniques have proved their efficacy for tasks like super-resolution (Da Wang et al., 2019; Bai & Berezovsky, 2020; Chen et al., 2020; Ahuja et al., 2022) and segmentation (Karimpouli & Tahmasebi, 2019; Y. Niu et al., 2020) in the workflow. However, applying DL for a denoising task has various challenges. The major barrier is the non-availability of clean images; hence, we do not have appropriate ground truth when using a supervised DL approach. Sidorenko et al. (2021) have used a supervised DL approach considering ground truth as images filtered using the bilateral filter followed by the band-pass filter. Unfortunately, this approach (Sidorenko et al., 2021) will inherently bias the DL model by the performance of the bilateral filter, therefore defeating the whole purpose of using DL as we could directly use a bilateral filter to perform the filtering. Another disadvantage of using the supervised DL approach is the requirement of a large dataset for training which itself is cumbersome. Also, creating an accurate dataset is very difficult as it requires inputs from various independent geologists and petrophysicists (Sidorenko et al., 2021).

To counteract the requirements of extensive training data and data curation, we can use the recently proposed unsupervised DL approaches (Laine et al., 2019; Lehtinen et al., 2018; Ulyanov et al., 2018) for denoising. Sidorenko et al. (2021) have demonstrated the efficacy of deep images prior to performing self-supervised denoising. However, all the self-supervised approaches are inherently slow as they require individual optimization for all the images to be denoised. Another disadvantage for most of these self-supervised approaches apart from their computational complexity (Sidorenko et al., 2021) is the unavailability of proper stopping criteria, making the implementation more time consuming and complex. Hence, there is a pressing need to develop a method/pipeline independent of data and a method/pipeline that is easy to optimize/tune. Our proposed pipeline is an amalgamation of two filtering techniques to denoise digital rock images.

This work proposes a novel denoising pipeline (Figure 1) that combines the advantage of morphology-based filtering (which relies on the shape of structural elements) with the NLM filtering. Herein, we consider a multi-resolution version of structurally varying bitonic filtering (Treece, 2016, 2019) for morphology-based filtering, which in short we refer to as MV-bitonic filtering. Since the morphology-based method is not based on pixel-based smoothing, edge preserving is achieved. Our proposed approach does not require training data, hence fast to implement in comparison to un-supervised DL approaches (Laine et al., 2019; Lehtinen et al., 2018; Ulyanov et al., 2018). Furthermore, the proposed pipeline is easy to tune and optimize in comparison to other existing

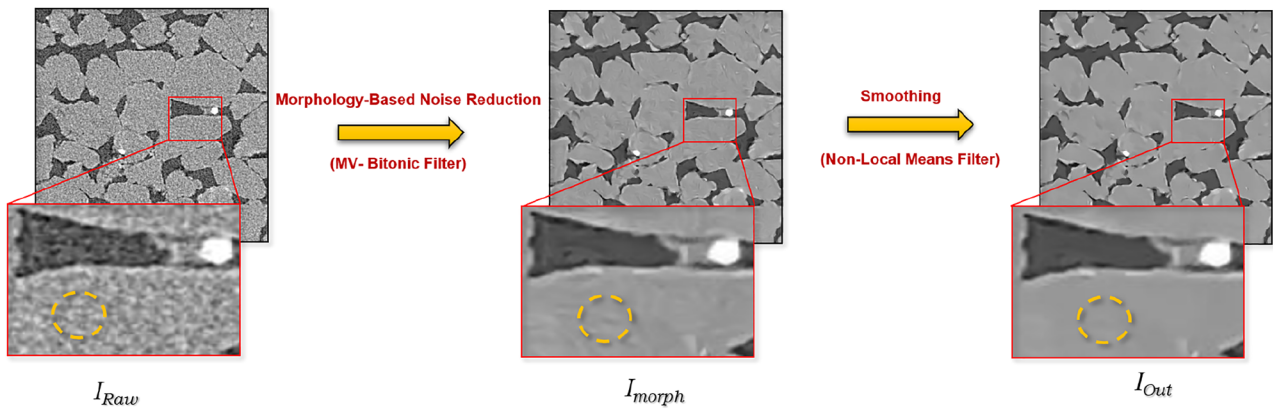


FIGURE 1 Proposed denoising pipeline using morphology-based noise reduction followed by non-local means filtering. The yellow circle shows efficient noise reduction for our proposed approach.

approaches. We show the efficacy of the proposed approach in terms of a non-reference metric (Kong et al., 2013) and also use the equivalent number of looks (ENL) (Shamsoddini et al., 2010) to incorporate geologists marking while calculating ENL which is proportional to the signal-to-noise ratio of significant regions in the filtered images. In addition to assessing the improvement using image-based evaluation metrics, we also examined the enhancement in two crucial petrophysical properties: porosity and permeability.

The structure of the paper is as follows: In the second section, the dataset description is provided and we explain the different image enhancement techniques, including NLM and MV-bitonic along with our proposed denoising pipeline. Furthermore, in the same section, the figures of merit outline the metrics utilized for the quantitative evaluation of various denoising methodologies in the paper. The results obtained by applying the aforementioned denoising methodologies, as well as their qualitative and quantitative evaluations, are presented in the third section. The implications of these results are briefly discussed in the fourth section. Finally, the conclusions of this study are presented in the last section.

MATERIALS AND METHODS

Dataset

Two-dimensional dataset: We consider two-dimensional (2D) slices of three different μ -CT scanned sandstones, namely BIM1 (Berea), CG2_12 (Castlegate) and FB24 (Fontainebleau). Also, these scans are acquired at two different resolutions (2 and 4 μm) using a Zeiss Xradia 520 versa scanner. Scans acquired at 2 μm tend to be more noisy compared to those acquired at 4 μm due to the presence of more high-frequency information. Hence, these scans can be used to evaluate the qualitative/quantitative differences among the various filters and the proposed approach; the same is demonstrated in the Results section.

Three-dimensional dataset: In this study, two open-source rock datasets (Ebadi, 2020; Sidorenko et al., 2021) (namely Rock A and Rock B) were used to evaluate various image enhancement methodologies. Porosity and permeability have been used as metrics for benchmarking these methodologies. The rocks in this dataset were scanned using the General Electric v-tome-x L240 CT system, specifically designed for imaging rocks of smaller dimensions. It is worth noting that the same dataset has been previously employed to benchmark different deep-learning-based denoising techniques (Sidorenko et al., 2021) in digital rock. Hence, we have chosen to use the same datasets to assess the performance of the denoising methodologies utilized in our work.

Image filtering techniques

This section describes various image enhancement techniques and our proposed pipeline in detail.

Non-local means filtering

Commonly used methods for image denoising are based on one common principle: efficient denoising can be achieved by just averaging the pixel intensities in the local neighbourhood. The Gaussian smoothing model (Lindenbaum et al., 1994), the anisotropic filtering (Perona & Malik, 1990) and the neighbourhood filtering (Yaroslavsky, 2012; Smith & Brady, 1997; Tomasi & Manduchi, 1998) are a few examples of denoising algorithms which perform local averaging of pixel intensities.

The non-local means (NLM) algorithm (Buades et al., 2005), instead of calculating the average pixel intensity in a local neighbourhood, takes a global approach to averaging. The NLM algorithm is based on the premise that all images have a degree of self-similarity which can be utilized

to denoise the image by averaging these self-similar parts (patches) in the image. In other words, most images will have similar patches in the image having similar noise characteristics across the image, which could be used for denoising these similar patches by averaging. Recently, NLM filtering has established itself as a standard pre-processing step (Andrä et al., 2013; Verri et al., 2017; Sell et al., 2016; Sun et al., 2017; Dong et al., 2020; Reshetova et al., 2020) in the digital rock workflow.

Multi-resolution structurally varying bitonic filtering

Treece (2016) proposed a bitonic filter that works on the concept of bitonicity. Any sequence is bitonic (Batcher, 1968) in nature if the sequence monotonically increases (or is constant) to its peak and thereafter monotonically decreases (or is constant). In simpler terms, any bitonic sequence will have a local minima/maxima or a saddle point. Most of the real signals can be considered as locally bitonic in a reasonably defined range; this encompasses both smooth signals and edges. Considering the above definition of bitonicity, we can define noise as any signal which is not bitonic in a given range (or bitonic over a shorter range). The above definition might be ambiguous if we consider impulsive (salt and pepper) noise, isolated impulses can be considered as signal as it follows the definition of bitonicity whereas multiple impulses in a given range will be considered as noise. The bitonic filter (Treece, 2016) was designed to preserve bitonicity in a given range and reject the rest. The bitonic filter combines robust morphological opening and closing operations with Gaussian filtering operators to remove the noisy (non-bitonicity) signal from the corrupted signal.

Since bitonicity is associated with the arrangement of values rather than actual values, it is pretty natural to switch to non-linear order-statistic/rank filtering. For 2D images to form a ranked set, we use a window which is commonly referred to as a ‘structuring element’ in morphology. The shape of the structuring element has a significant impact on the features that can be preserved (Treece, 2016). In the case of a bitonic filter, a circular mask was employed to maintain an isotropic behaviour while denoising. The bitonic filter is shown to outperform most of the filters except the NLM filter in terms of signal-to-noise (SNR) performance (Treece, 2016).

Recently, a more robust version of bitonic filtering incorporating structurally varying morphological operation (also called adaptive morphology; Landström & Thurley, 2013) was proposed by Treece (2016). It also incorporates data thresholds and morphological operation, promoting further noise reduction and implementing a multi-resolution frame-

work for filtering. MV-Bitonic filtering shows considerable improvement over NLM, and hence we incorporate the same in our proposed denoising pipeline for the digital rock workflow. The working of MV-bitonic filtering can be found in detail in Treece (2019).

Proposed filtering pipeline

NLM filtering has established itself as the state-of-the-art technique for denoising the digital rock workflow. Note that the performance of NLM filtering can be further enhanced to get more optimal segmentation when the noise in the reconstructed volumes is high. Recently, MV-bitonic filtering is proposed for denoising and is shown to outperform NLM at almost all noise levels (Treece, 2019). MV-Bitonic, on the other hand, has a problem of inefficient denoising in regions expected to have constant intensities in the image and is more prominent in images having high noise, that is, images at a higher resolution. Hence, in this work, we propose a denoising pipeline to compensate for the degradation in the performance of NLM filtering at a higher noise level (which is when images are acquired at a higher resolution) and residual noise in MV-bitonic filtering (regions having constant pixel intensities).

This work proposes a novel denoising pipeline consisting of morphology-based noise reduction using MV-bitonic filtering, followed by NLM smoothing. Initially, morphological operations are used to reduce noise which is then followed by NLM smoothing. This procedure could help us in achieving edge-preserving smoothing by combining the best of both worlds (NLM and bitonicity). Edge-preserved enhancement could help in achieving optimal segmentation using a basic segmentation algorithm like Otsu thresholding (Otsu, 1979). Mathematical details of our proposed pipeline are presented below.

Morphological operations namely robust opening $\mathbf{O}_{w,c}$ and closing $\mathbf{C}_{w,c}$ applied on image $I_{\text{raw}}(p)$ at location p can be written as

$$\mathbf{R}_{w,c}(I_{\text{raw}}(p)) = c^{\text{th centile}}_{y \in w} \{I_{\text{raw}}(p + y)\}, \quad (1)$$

$$\mathbf{O}_{w,c} = \mathbf{R}_{w,100-c}(\mathbf{R}_{w,c}(I_{\text{raw}}(p))), \quad (2)$$

$$\mathbf{C}_{w,c} = \mathbf{R}_{w,c}(\mathbf{R}_{w,100-c}(I_{\text{raw}}(p))), \quad (3)$$

where $\mathbf{R}_{w,c}$ is a rank filter and y is the vector distance to a location close to p within the region w (which here is a 2D structurally varying structuring element) with a pre-chosen

centile c (which here is assumed as 4% for optimal filter performance). Rank filter sorts (ranks) I_{raw} over w and returns the pixel value corresponding to the chosen centile c . Note that $\mathbf{O}_{w,c}$ and $\mathbf{C}_{w,c}$ operations are meant to preserve local minima or local maxima only and also these operations do not preserve the mean intensity of the signal. To remove these defects, we weigh these operations as described below:

$$\epsilon_O = \|\mathbf{G}_{\sigma,\alpha}(I_{\text{raw}} - \mathbf{O}_{w,c})\|, \quad (4)$$

$$\epsilon_C = \|\mathbf{G}_{\sigma,\alpha}(\mathbf{C}_{w,c} - I_{\text{raw}})\|, \quad (5)$$

$$\mathbf{I}_{\text{morph}_{w,c}} = \frac{\epsilon_O^m(\mathbf{C}_{w,c} - \epsilon_C) + \epsilon_C^m(\mathbf{O}_{w,c} + \epsilon_O)}{\epsilon_O^m + \epsilon_C^m}, \quad (6)$$

where ϵ_O and ϵ_C represent the smoothed version of the errors obtained after subtracting $\mathbf{O}_{w,c}$ and $\mathbf{C}_{w,c}$ from the original image I_{raw} and $\mathbf{I}_{\text{morph}_{w,c}}$ is the output of the structurally varying bitonic filter. In Equation (6), m controls the transition between the opening and the closing operation. Setting m as 3 gives a more sudden transition between the morphological operation, which slightly improves the performance (Treece, 2019) and hence has been a default choice for our experiments. $\mathbf{G}_{\sigma,\alpha}$ represents Gaussian-like filtering which depends on the ϕ representing the angle which follows the dominant features direction in the image and γ representing the degree of anisotropy. ϕ and γ can be derived using the well-known structure tensor \mathbf{T} as shown below:

$$\mathbf{T} = \begin{bmatrix} G_\sigma(g_x^2) & 2G_\sigma(g_x g_y) \\ 2G_\sigma(g_x g_y) & G_\sigma(g_y^2) \end{bmatrix} = \begin{bmatrix} T_{xx} & T_{xy} \\ T_{xy} & T_{yy} \end{bmatrix}, \quad (7)$$

where g_x and g_y represent the gradients in horizontal \mathbf{x} and vertical direction \mathbf{y} of the image $I_{\text{raw}}(p)$ while G_σ represents the Gaussian smoothing. The local direction $\phi(p)$ and degree of anisotropy $\gamma(p)$ are calculated using the eigenvalues $\lambda_{1,2}$ of \mathbf{T} calculated at the current pixel location p in the image I_{raw} and is given by

$$\lambda_{1,2} = \frac{1}{2} \left(T_{xx} + T_{yy} \pm \sqrt{(T_{xx} - T_{yy})^2 + T_{xy}^2} \right), \quad (8)$$

$$\gamma(p) = 1 - \frac{\lambda_2}{\lambda_1}, \quad (9)$$

$$\phi(p) = \frac{1}{2} \tan^{-1} \left(\frac{T_{xy}}{T_{xx} - T_{yy}} \right). \quad (10)$$

Using γ and ϕ , we calculate the expression for Gaussian-like smoothing $\mathbf{G}_{\sigma,\alpha}$ as

$$D_q(p) = |q \sin(\angle(q) - \phi(p))|, \quad (11)$$

$$\Psi_q(p) = \frac{e^{-\frac{|q|^2}{2\sigma^2}}}{\left(\frac{D_q(p)\gamma(p)^2}{\alpha^2} + 1 \right) \left(\frac{D_q(p+q)\gamma(p+q)^2}{\alpha^2} + 1 \right)}, \quad (12)$$

$$\mathbf{G}_{\sigma,\alpha} = \frac{\sum_{q \in w_l} \Psi_q(p) I_{\text{raw}}(p+q)}{\sum_{q \in w_l} \Psi_q(p)}, \quad (13)$$

where p represents the current pixel location and q represents the vector distance to the neighbouring location in the rectangular window w_l of size $l \times l$. $\mathbf{G}_{\sigma,\alpha}$ represents the smoothing via weighted average as shown in Equation (13). Weights (Equation 12) being used are dependent on the dominant image direction $D_q(p)$, anisotropy γ and α , which capture the overall effect of anisotropy. If $\alpha \gg 1$, $\mathbf{G}_{\sigma,\alpha}$ reduces simply to Gaussian filtering \mathbf{G}_σ . Optimal sets of masks and their optimal orientation are obtained to implement morphological operations as defined in Treece (2019). Using a set of operations defined from Equation (1) to Equation (6), we morphologically denoise I_{raw} to obtain I_{morph} which completes the first step of our proposed pipeline.

In the second step of our pipeline, we aim to improve the output of morphological filtering (Treece, 2019) indicated as I_{morph} . This is achieved by applying NLM smoothing operation on I_{morph} . Given residual noise in the corrupted image (i.e., inefficient denoising using morphological filtering) $\{r(p)|p \text{ is the pixel location in image } I_{\text{morph}}\}$, the estimated value $I_{\text{out}}[r](p)$ using NLM filtering at pixel location p is given as

$$I_{\text{out}}[r](p) = \sum_{j \in I_{\text{morph}}} w(p, j) r(j), \quad (14)$$

we observe that in order to estimate a pixel value at location p we require information of all the pixels in image I_{morph} . In Equation (14), the family of weights $w(p, j)$ depends on the similarity between the pixel at location p and j . The weight is directly proportional to the similarity in the intensities of grey levels between the pixel pair. Mathematically, $w(p, j)$ is defined as

$$w(p, j) = \frac{1}{Z(p)} e^{-\frac{\|\mathbf{r}(\mathcal{N}_p) - \mathbf{r}(\mathcal{N}_j)\|_2^2}{h^2}}, \quad (15)$$

where $\mathbf{r}(\mathcal{N}_k)$ denotes a vector calculated from a fixed square neighbourhood \mathcal{N}_k centred at pixel location k . Here,

TABLE 1 Comparison of various metrics used for quantitative evaluation across various denoising methods.

Metrics	Input	Role
Kong et al. (2013)	Complete 2D Slice	Quantifies overall image quality (edge preservation and efficient denoising in Homogeneous regions)
ENL	Marked ROIs	Quantifies structure preservation while denoising
Porosity	Complete 3D Volume	Quantifies overall efficacy of digital rock pipeline to predict various petrophysical properties
Permeability	Complete 3D Volume	Quantifies overall efficacy of digital rock pipeline to predict various petrophysical properties

Abbreviations: 2D, two- dimensional; 3D, three-dimensional; ROI, regions of interest.

similarity is measured using the weighted Euclidean distance $\|\mathbf{r}(\mathcal{N}_p) - \mathbf{r}(\mathcal{N}_j)\|_2^2$ and $Z(p)$ is the normalization constant defined as

$$rmZ(p) = \sum_j e^{-\frac{\|\mathbf{r}(\mathcal{N}_p) - \mathbf{r}(\mathcal{N}_j)\|_2^2}{h^2}}, \quad (16)$$

where h is the degree of filtering. Equations (14)–(16) are the steps involved in performing NLM denoising of I_{morph} to obtain the final denoised image I_{out} .

Figures of merit

The major bottleneck involved in coming up with a proper pre-processing pipeline for digital rock is the unavailability of the ground truth images, making it challenging to quantify various denoising algorithms. Therefore, we use the non-reference metric proposed by Kong et al. (2013), which was recently used to quantify the digital rock images (Sidorenko et al., 2021). We also use the equivalent number of looks (ENL) (Shamsoddini et al., 2010) to incorporate geologists marking while computing the SNR of different important regions in the filtered images. Moreover, we also compute porosity and permeability on the 3D dataset for comparison. Table 1 clearly explains the utility of different figures of

metrics. It illustrates the specific usage of each metric. Out of the four metrics, one metric utilizes regions of interest (ROIs) marked by geologists, another metric operates on the entire slice, and the remaining metrics work with the complete 3D volume.

Non-reference metric

Kong et al. (2013) proposed a relatively simple non-reference metric. The structural similarity index (SSIM) (Z. Wang et al., 2004) maps are used for capturing structural similarity, and the detailed steps are presented below:

1. Calculate method noise image $I_{\text{noise}}: I_{\text{raw}} - I_{\text{out}}$.
2. Calculate the SSIM map (M) between I_{noise} and I_{raw} .
3. Calculate the SSIM map (N) between I_{out} and I_{raw} .
4. Image quality score (s): Pearson's linear correlation coefficient between SSIM maps M and N .

Step 2 is used to understand how accurately the homogeneous regions in the rock images are denoised, while Step 3 indicates how accurately the highly structured regions are preserved.

Equivalent number of looks

In order to quantify how well the homogeneous regions of the image are denoised, we used the ENL metric, which has been widely used in the literature (Shamsoddini et al., 2010; Gong et al., 2015; X. Wang et al., 2012; Mohan et al., 2021) in the context of speckle noise removal. Mathematically, the ENL is defined as below:

$$\text{ENL}_{\text{ROI}} = \frac{\mu_{\text{ROI}}^2}{\sigma_{\text{ROI}}^2}, \quad (17)$$

where μ_{ROI} and σ_{ROI} represent the mean and standard deviation of the selected region of interest. The higher is the value of ENL, the higher is the efficacy of the filter to remove noise in the homogeneous region (grain and pore regions for digital rock images). Furthermore, the SNR has a direct correlation to ENL values.

Porosity

Porous media is composed of two phases: the solid phase and the pore phase. The solid phase consists of various materials, while the pore phase represents the empty space within the media. The total porosity is a measure defined as the ratio

of the total pore space volume to the total volume of the porous media. We estimate the porosity from the segmented 3D volume. There are many methods described in the literature to estimate the image-based porosity (Withjack, 1988; Akin et al., 1996; Taud et al., 2005; Schepp et al., 2020). We have used the adaptive thresholding segmentation technique (Bradley & Roth, 2007) on the outputs produced from each denoising methodology. We used the same hyper-parameters for performing adaptive thresholding across all the different denoising methods for consistency.

Permeability

Permeability is another widely used figure of metric to assess the performance of digital rock pipelines. It plays a crucial role in assessing porous geological samples for various applications, including water management, fluid recovery and carbon dioxide sequestration (Su et al., 2019; Q. Niu & Zhang, 2019; Zhang et al., 2020; Millington & Quirk, 1961; C. F. Berg and Held, 2016). Recently, several studies (Liu et al., 2023; Jiang et al., 2023; Liao et al., 2023; Payton et al., 2022) have efficiently estimated permeability from digital rocks. In our study, we have employed a recent study that offers insights into the relationship between porosity and permeability in sandstone reservoirs (Payton et al., 2022). By utilizing the Kozeny–Carman equation, Payton et al. (2022) derived the relationship as $K = 10^{5.68} \phi^{3.88}$, where K represents permeability and ϕ represents porosity.

RESULTS

We have reported the results from three different rocks acquired at two different resolutions. The different denoising parameters corresponding to different filtering approaches were chosen heuristically to result in maximum image quality score s defined in the Non-local means filtering section. Note that the resulting parameters were optimal in relation to the image quality score s . Parameters used for tuning various filters are mentioned as follows:

- *Non-local means (NLM) filtering*: We optimally choose the *degree of smoothing* and *search window size*.
- *Multi-resolution structurally varying (MV-Bitonic) filtering*: We optimally choose r , which represents the maximum radius of the structurally varying masks.
- *Proposed denoising pipeline*: We optimally choose r for morphological filtering in Step 1 and *degree of smoothing* in Step 2.

Qualitative results: For qualitative comparison, we have considered the optimality of the segmentation algorithm, which

TABLE 2 Comparison of different denoising methods utilized in this work in terms of a non-reference metric (Kong et al., 2013). The best performing method is shown in bold.

Rock	NLM	MV-bitonic	Proposed
B1M1 (2 μm)	0.7169	0.7098	0.7294
CG2_12 (2 μm)	0.7082	0.7224	0.7500
FB24M2 (2 μm)	0.5711	0.6362	0.6901
B1M1 (4 μm)	0.7158	0.7215	0.7329
CG2_12 (4 μm)	0.7621	0.7821	0.7934
FB24M2 (4 μm)	0.7252	0.7298	0.7901

Abbreviations: MV-bitonic, multi-resolution structurally varying bitonic; NLM, non-local means.

is the next step in the digital rock workflow. Furthermore, we have chosen a simpler segmentation algorithm, namely Otsu thresholding (Otsu, 1979), to evaluate the differences between the performance of different filters and our proposed denoising pipeline. Figures 2(i) and 3(i) show the visual performance of various filters and the proposed denoising pipeline corresponding to 2 and 4 μm resolution, respectively. Figures 2(ii) and 3(ii) bring out differences in the segmentation performance of various filters and the proposed denoising pipeline. The yellow arrows in these figures indicate the visual differences between the various denoising methods and with original raw reconstructed output. As expected, images acquired at a higher resolution tend to be noisier; hence, visual differences in the segmented images can be easily observed in the images scanned at a higher resolution (as shown in Figure 2). Our proposed pipeline tends to provide the optimal segmentation in comparison to other filters, and yellow arrows are used to indicate the same in Figures 2 and 3. In order to make a qualitative comparison of rock volumes, it is necessary to expand our pipeline to accommodate and process 3D images. Our approach involves analysing entire 3D volumes by applying the proposed pipeline to each individual slice and then combining them to obtain a fully denoised 3D volume. We have provided a visual comparison for Rock A (Figure 4).

Quantitative results: Apart from the qualitative study, we evaluated the performance of different filtering approaches quantitatively. Initially, the non-reference metric (see the Non-reference metric section) was computed for the different denoised rocks; note that the non-reference metric considers all the required conditions necessary for performing edge-preserving denoising. We also quantify the different image enhancement approaches using the equivalent number of looks (ENL). ENL indicates how accurately the homogeneous regions of the rocks (i.e., pores or grains) are denoised. For digital rock images, we compute ENL separately for the grain and pore region using the representative region marked by a geologist for each rock as indicated in Figure 5. Tables 2–4 show the quantitative comparison using a non-reference

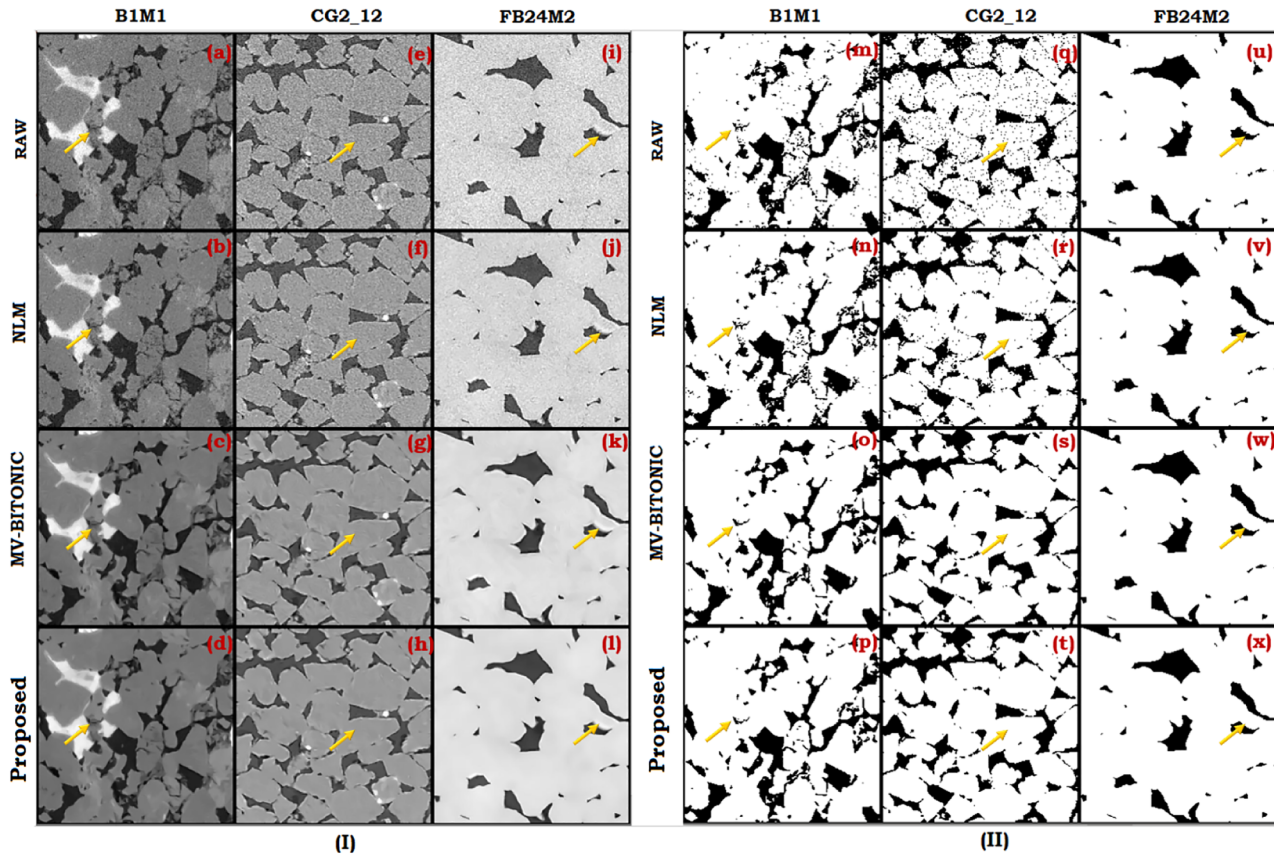


FIGURE 2 Visual results for all three rocks B1M1, CG2_12 and FB24 acquired at 2 μm resolution. (I) presents raw, NLM, MV-bitonic, and proposed images, respectively, arranged along the rows. (II) presents segmented images using the Otsu algorithm (Otsu, 1979) for raw, NLM, MV-bitonic and proposed images, respectively, arranged along the rows. Yellow arrows indicate the efficacy of our proposed approach in terms of optimality of the segmented image. MV-bitonic, multi-resolution structurally varying bitonic; NLM, non-local means.

TABLE 3 Comparison of different denoising methods utilized in this work in terms of an ENL calculated for grain using the ROI marked (by a petrologist/geologist) as shown in Figure 5. The best performing method is shown in bold. All values for ENL are reported in the order of 10^3 .

Rock	Raw	NLM	MV-bitonic	Proposed
B1M1 (2 μm)	0.1323	0.3236	1.9040	4.1991
CG2_12 (2 μm)	0.0686	0.1710	1.6707	3.7299
FB24M2 (2 μm)	0.1810	0.5267	7.9685	12.1598
B1M1 (4 μm)	0.9923	4.9370	7.0818	9.0374
CG2_12 (4 μm)	0.3669	1.6881	2.7681	7.0155
FB24M2 (4 μm)	0.4986	1.8568	2.3553	43.5399

Abbreviations: ENL, equivalent number of looks; MV-bitonic, multi-resolution structurally varying bitonic; NLM, non-local means.

metric and ENL for grain and pore regions, respectively. The obtained quantitative value (shown in the tables) indicates that our proposed pipeline outperforms the state-of-the-art non-local means (NLM) filtering. Further, the obtained quantitative values are higher in the 4- μm case compared to

TABLE 4 Comparison of different denoising methods utilized in this work in terms of an ENL calculated for the pore region using the ROI marked (by a petrologist/geologist) as shown in Figure 5. The best performing method is shown in bold. All values for ENL are reported in the order of 10^3 .

Rock	Raw	NLM	MV-bitonic	Proposed
B1M1 (2 μm)	0.0192	0.0518	0.0992	0.2405
CG2_12 (2 μm)	0.0182	0.0408	0.1224	0.3114
FB24M2 (2 μm)	0.0271	0.0954	0.9973	2.8572
B1M1 (4 μm)	0.2200	0.6776	0.7506	2.2260
CG2_12 (4 μm)	0.0598	0.0896	0.1455	0.3367
FB24M2 (4 μm)	0.0339	0.1061	0.1723	3.8992

Abbreviations: ENL, equivalent number of looks; MV-bitonic, multi-resolution structurally varying bitonic; NLM, non-local means.

the 2- μm case since the 4- μm acquisition is less noisy in comparison to the 2- μm acquisition.

We also employed a three-dimensional (3D) dataset (rock volume A and rock volume B) to perform an estimation of the porosity using the adaptive segmentation technique (Bradley & Roth, 2007). To facilitate a quantitative

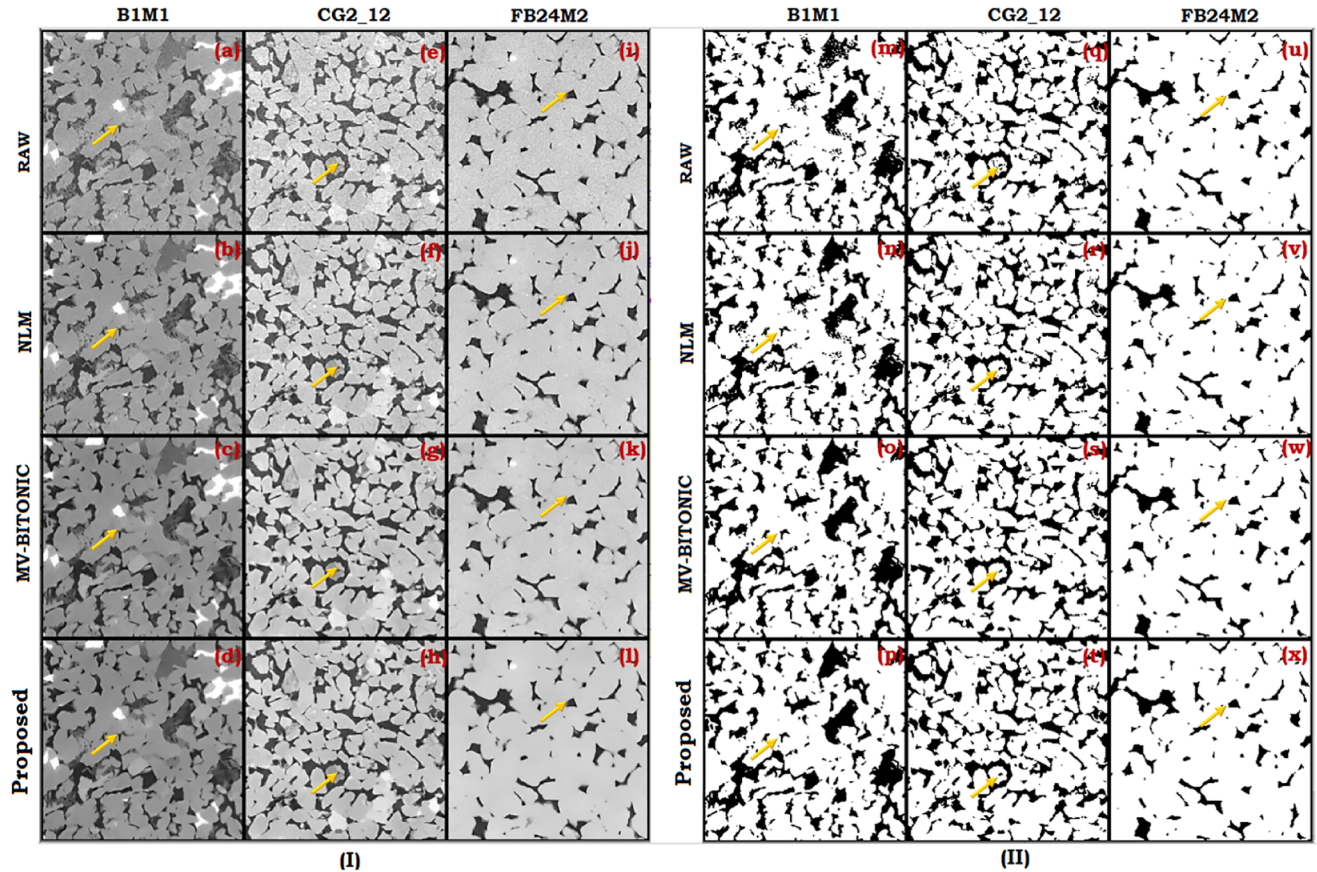


FIGURE 3 Visual results for all the three rocks B1M1, CG2_12 and FB24 acquired at 4 μm resolution. (I) presents raw, NLM, MV-bitonic and proposed images arranged along the rows, respectively. (II) presents segmented images using the Otsu algorithm (Otsu, 1979) for raw, NLM, MV-bitonic and proposed images arranged along the rows, respectively. Yellow arrows indicate the efficacy of our proposed approach in terms of the optimality of segmented images. MV-bitonic, multi-resolution structurally varying bitonic; NLM, non-local means.

TABLE 5 Comparison of various denoising methods in terms of estimated porosity for Rock A and Rock B. Closest porosity values to the reference porosity are shown in bold. We also include percentage absolute error for the estimated porosity considering reference porosity as baseline. Reference values were computed using benchmark volumes provided by Sidorenko et al. (2021) and Ebadi (2020).

Method	Rock A (reference porosity: 16.17 p.u.)	Rock B (reference porosity: 18.30 p.u.)
	Porosity (p.u.) / absolute error (%)	Porosity (p.u.) / absolute error (%)
Raw	31.17 / 92.76	31.87 / 74.15
NLM	12.43 / 23.13	14.60 / 20.21
MV-Bitonic	13.77 / 14.84	16.19 / 11.53
Proposed	14.49 / 10.38	16.78 / 8.30

Abbreviations: MV-bitonic, multi-resolution structurally varying bitonic; NLM, non-local means.

comparison, we have utilized the reference benchmark volumes provided by Sidorenko et al. (2021). The image enhancement techniques that produced the porosity estimate closest to the reference porosity were identified as the top-performing denoising methodology. Table 5 displays the estimated porosity values and the corresponding percentage absolute errors (computed using the reference porosity

as the baseline) for the denoised rock volumes A and B. The analysis clearly demonstrates that our proposed denoising pipeline exhibits the lowest absolute error in porosity estimation compared to the other denoising model.

Notably, the enhancements achieved through our proposed denoising pipeline are not limited solely to porosity estimation. The improvements were found to extend to subsequent

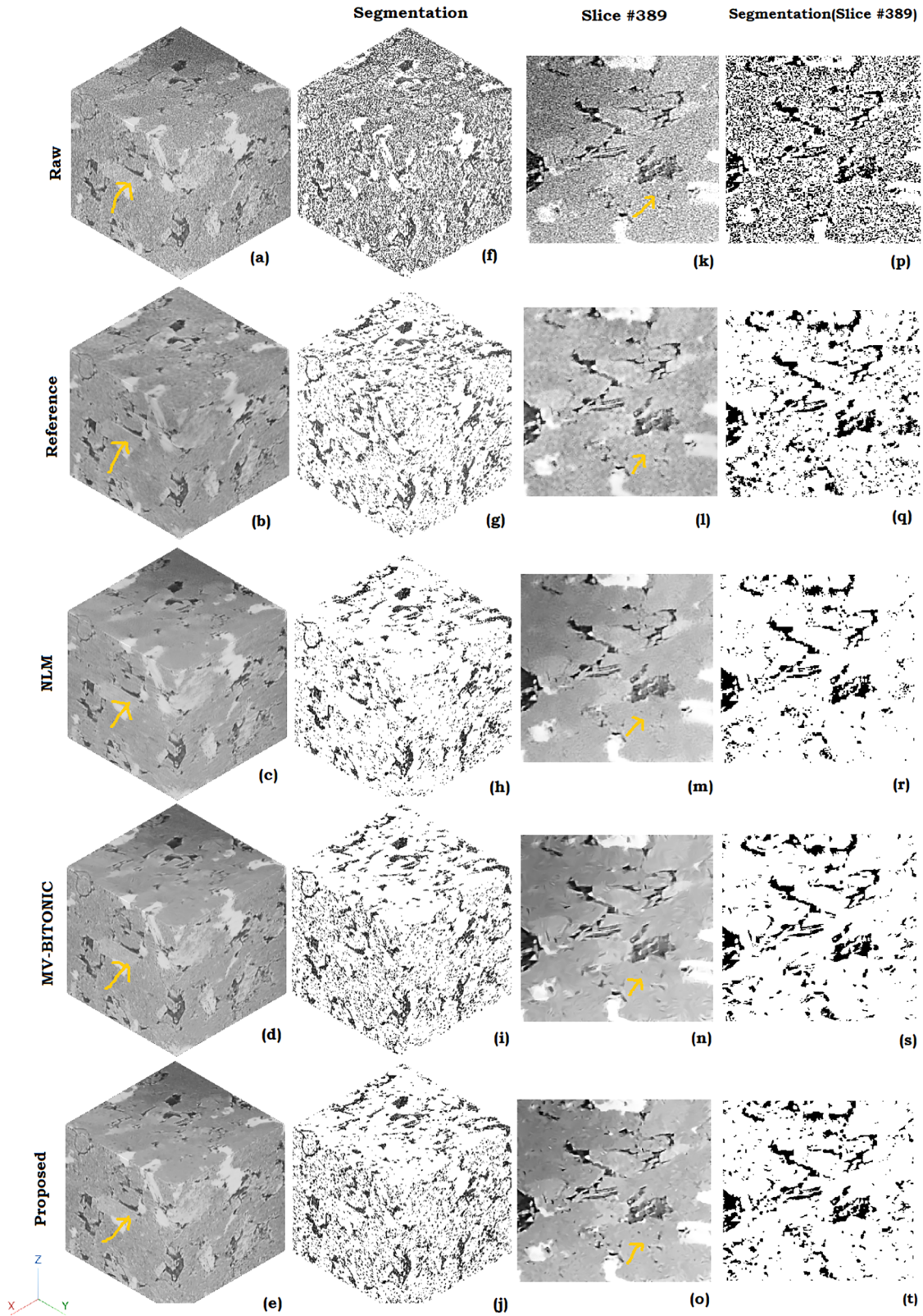


FIGURE 4 Visual results for rock volume A. It represents raw, reference, NLM, MV-bitonic and proposed volumes along with a representative 2D slice for each method arranged along the rows. We also include segmented results (3D and 2D) for raw, reference, NLM, MV-bitonic and proposed arranged along the rows, respectively.

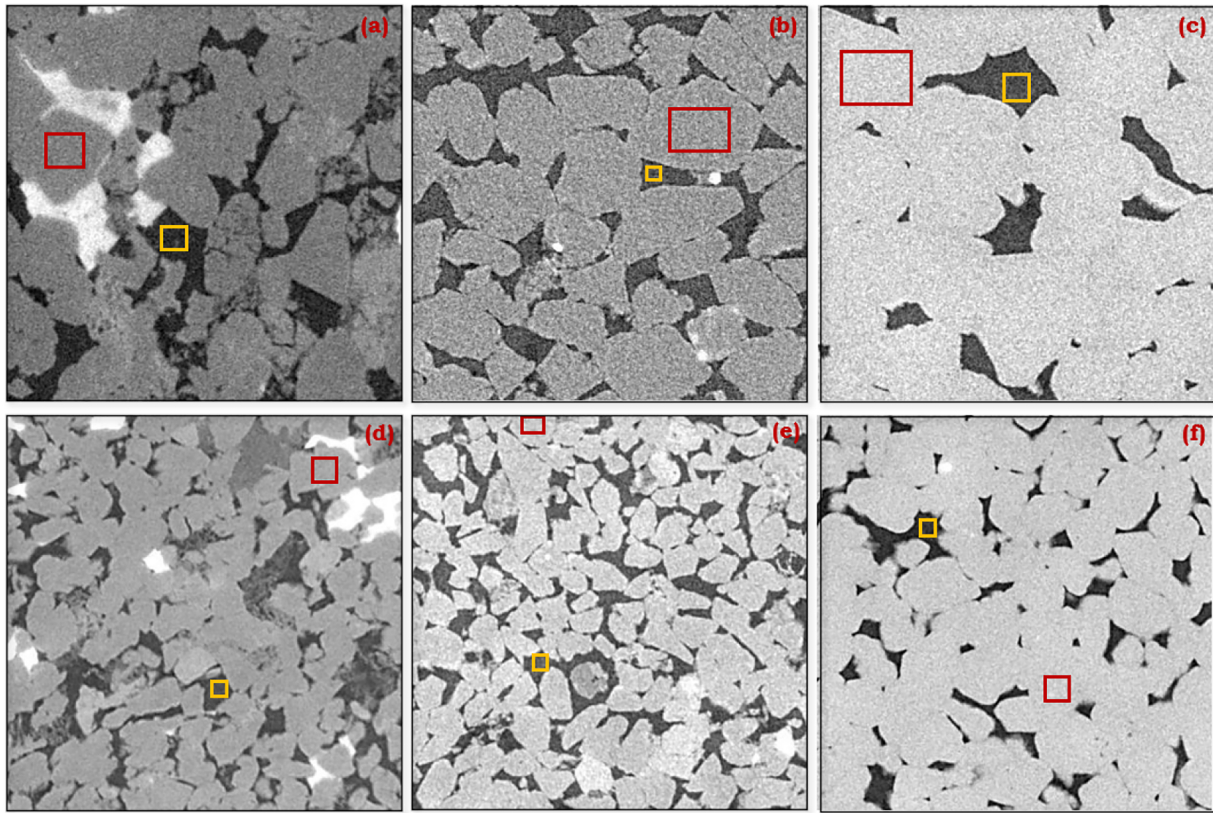


FIGURE 5 Various marked regions of interest (ROI) by petrologists/geologists for all the six images considered for our study. These marked ROIs are used to calculate the equivalent number of looks (ENL) for both grain and pore regions. The red ROI represents the grain region, while the yellow ROI represents the pore region. (a) B1M1 (2 μm), (b) CG2_12 (2 μm), (c) FB24 (2 μm), (d) B1M1 (4 μm), (e) CG2_12 (4 μm) and (f) FB24 (4 μm).

TABLE 6 Estimated permeabilities for rock samples A and B across different denoising methods. The closest permeability value to the reference absolute permeability is shown in bold. We also include percentage error for the estimated permeabilities considering reference permeability as baseline. Reference values were computed using benchmark volumes provided by Sidorenko et al. (2021) and Ebadi (2020).

Method	Rock A (reference permeability: 407.42 mD)	Rock-B (reference permeability: 658.73 mD)
	Permeability (mD)/absolute error (%)	Permeability (mD)/absolute error (%)
Raw	5.19e+3 / 1173.86	5.67e+3 / 760.75
NLM	146.66 / 64.00	274.29 / 58.36
MV-Bitonic	218.49 / 46.37	409.47 / 37.84
Proposed	266.24 / 34.65	469.62 / 28.71

Abbreviations: ENL, equivalent number of looks; MV-bitonic, multi-resolution structurally varying bitonic; NLM, non-local means.

stages in the digital rock workflow, we have also performed permeability estimation across all denoising methodologies. In Table 6, the estimated permeability values for rock volumes A and B are summarized, along with the corresponding absolute error percentages. It is evident that our proposed pipeline achieves the lowest error in permeability estimation compared to all other methodologies discussed. The results are also depicted using absolute error plots (in Figure 6), highlighting the magnitude of difference observed while mea-

suring both porosity and permeability across the different denoising methodologies.

Computationally, our proposed pipeline takes more time than individually applied NLM and MV-bitonic filtering. For example, NLM takes 0.206 s, MV-bitonic takes 1.395 s, while our proposed method takes 2.973 s for denoising a 400×400 slice of a Fontainebleau rock acquired at 4 μm . However, at the same time, we get superior performance in terms of a non-reference metric and a significant boost in the value of

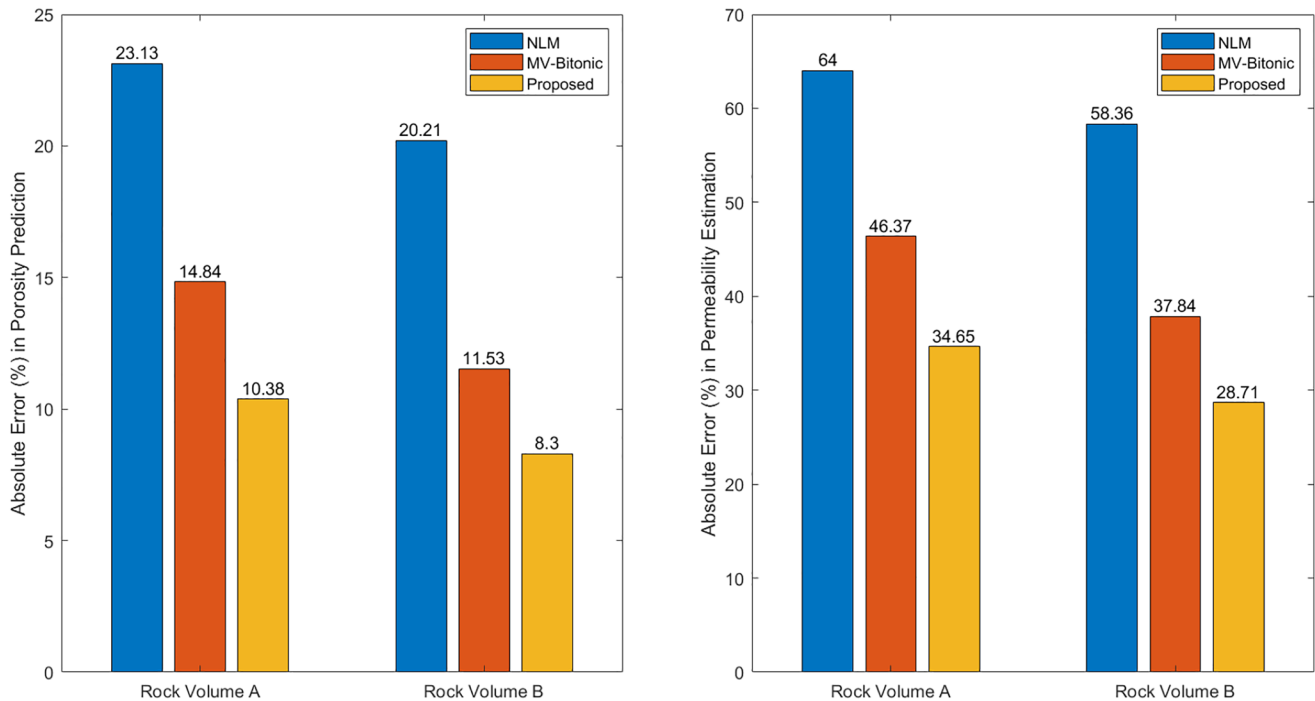


FIGURE 6 Results presented in the form of absolute error plots, which visually illustrate the magnitude of differences in measuring petrophysical parameters (porosity and permeability). The estimation of porosity and permeability values was conducted using segmented rock volumes of A and B, employing different denoising methodologies.

ENL, which indicates significant homogeneity in the constant regions (grain and pore region).

DISCUSSION

In our proposed denoising pipeline, we have integrated a crucial component called the multi-resolution structurally varying bitonic filter (MV-bitonic). This filter plays a vital role in reducing noise. One of its significant advantages is its ability to dynamically adjust its shape based on the noise characteristics present in the image (Treece, 2016, 2019). This unique adaptability sets it apart from other filters like Gaussian, mean, median and other ones that lack this property. Additionally, these filters are prone to introducing smoothing artefacts due to their inherent implementation (visual comparison presented in Figure 7). In contrast, the inclusion of the bitonic filter in our pipeline aids in preserving finer details and minimizing the smoothing of essential rock features. As a result, it indirectly contributes to the accurate estimation of various petrophysical parameters, such as porosity and permeability, within the digital rock pipeline.

The key step involved in our pipeline is morphology-based noise reduction, which reduces the noise using adaptive opening and closing operations. Preserving edges along with

smoothing out the homogeneous region is a challenging task. Hence, our approach has incorporated morphological operation, which significantly reduces noise in the input image while preserving edges. An important drawback of using the bitonic filter and its variants is the presence of residual noise in the homogeneous regions (i.e., grain and pores) leading to heterogeneous regions in these regions which could adversely affect the physical simulation results. To counteract this, we have performed a non-local smoothing on top of the morphologically denoised image to smoothen out the homogeneous region, leading to a significant boost in the performance, that is, getting a higher number for the equivalent number of looks in the pore as well as grain regions of the image. It is emphasized that the additional step of non-local filtering requires minimal tuning as the majority of the high-intensity noise has already been removed through multi-resolution structurally varying bitonic filtering. Furthermore, incorporating non-local smoothing as the final step also gives us an improved non-reference metric, indicating efficient structure-preserving denoising characteristics. Moreover, it is worth highlighting that our proposed approach not only demonstrates effectiveness in image-based evaluation but also significantly enhances the accuracy of estimating petrophysical parameters, specifically porosity and permeability, within the workflow.

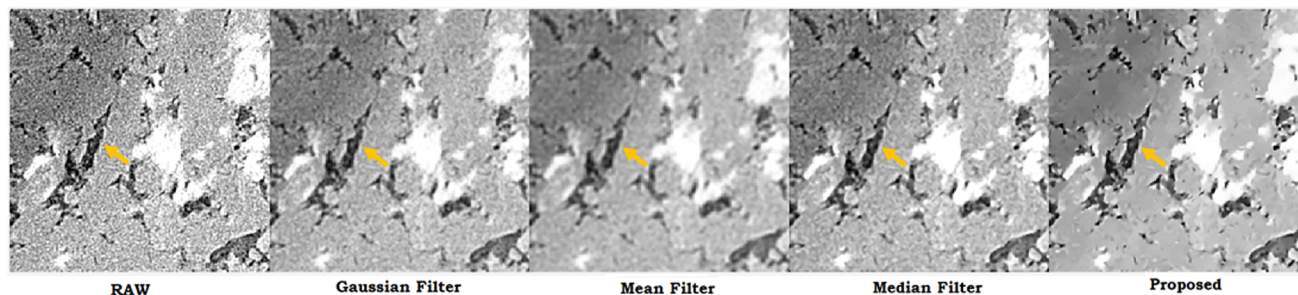


FIGURE 7 Visual comparison of our proposed pipeline with Gaussian, mean and median filtering techniques. It is evident that our methodology outperforms the others in terms of efficient edge preservation and minimal presence of smoothing artefacts during denoising.

CONCLUSION

This work proposes a novel pipeline to efficiently denoise digital rock images before performing image segmentation and physics-based simulation. The pipeline combines non-local means (NLM) smoothing with the morphological operation. Quantitative metrics like the equivalent number of looks (ENL) calculation for grains and pores and a non-reference metric indicating edge-preserving denoising were found to be superior compared to the NLM and multi-resolution structurally varying (MV-bitonic) filtering. The improvement attained through the proposed denoising pipeline in terms of the non-reference metric is as high as 20.8% when compared to the most widely used the NLM filtering approach. Moreover, the proposed pipeline provides a minimum improvement of 9.1 \times for ENL(grains) and 5.6 \times for ENL (pores) in comparison to the raw acquisition. In contrast, the NLM filter could only provide a maximum improvement of 4.9 \times for ENL (grains) and 3.5 \times for ENL (pores) with respect to noisy samples. The Fontainebleau (4 μ m) rock sample being the least noisy acquisition provides the maximum improvement of 87 \times for ENL (grains) and 115 \times for ENL (pores) when denoised using the proposed pipeline in comparison to raw images. Furthermore, visual inspection of the segmented image showed the qualitative efficacy of the proposed method over individually applied NML or morphological procedures. Moreover, our proposed pipeline demonstrates significant accuracy in estimating porosity. It achieves the lowest absolute error percentages of 10.38% and 8.3% for rock volumes A and B, respectively. In contrast, the NLM-filtered volume exhibits significantly higher error percentages of 23.13% and 20.21% for Rocks A and B, respectively. This same trend holds true for permeability estimation, where our proposed pipeline outperforms both MV-bitonic filtering and NLM filtering, with the least absolute error percentages of 34.65% (Rock A) and 28.71% (Rock B).

ACKNOWLEDGEMENTS

The authors thank Shell International Exploration and Production Inc. for permission to publish this work. They would

like to thank especially Justin Freeman, Kunj Tandon, Stefan Berg, F. O. Alpak, Bochao Zhao, and Chaitanya Pradhan for discussions and Pandu Devarakota for his critical review, which significantly improved the paper.

DATA AVAILABILITY STATEMENT

The two-dimensional imaging data utilized in this work are available from the corresponding author upon reasonable request. The three-dimensional dataset (rock A and rock B) is available as open source (Ebadi, 2020).

CODE AVAILABILITY STATEMENT

Implementation of morphological filtering has been done based on a publicly available code at <https://in.mathworks.com/matlabcentral/fileexchange/68541-structurally-varying-bitonic-filter>. Non-local mean filtering is performed using default Matlab functionality (imnlmfilt function in Matlab).

ORCID

Phaneendra K. Yalavarthy  <https://orcid.org/0000-0003-4810-352X>

REFERENCES

- Ahuja, V.R., Gupta, U., Rapole, S.R., Saxena, N., Hofmann, R., Day-Stirrat, R.J., Prakash, J. & Yalavarthy, P.K. (2022) Siamese-sr: a Siamese super-resolution model for boosting resolution of digital rock images for improved petrophysical property estimation. *IEEE Transactions on Image Processing*, 31, 3479–3493.
- Akin, S., Demiral, M. & Okandan, E. (1996) A novel method of porosity measurement utilizing computerized tomography. *In situ*, 20(4), 347–365.
- Al-Marzouqi, H. (2018) Digital rock physics: using CT scans to compute rock properties. *IEEE Signal Processing Magazine*, 35(2), 121–131.
- Andrä, H., Combaret, N., Dvorkin, J., Glatt, E., Han, J., Kabel, M., Keehm, Y., Krzikalla, F., Lee, M., Madonna, C., et al. (2013) Digital rock physics benchmarks-Part I: Imaging and segmentation. *Computers & Geosciences*, 50, 25–32.
- Bai, Y. & Berezovsky, V. (2020) Digital rock core images resolution enhancement with improved super-resolution convolutional neural networks. In *Proceedings of the 2020 12th International Conference on Machine Learning and Computing*. New York: ACM, pp. 401–405.

- Batcher, K.E. (1968) Sorting networks and their applications. In *Proceedings of the April 30–May 2, 1968, Spring Joint Computer Conference*, AFIPS '68 (Spring). New York: Association for Computing Machinery, pp. 307–314.
- Berg, C.F. & Held, R. (2016) Fundamental transport property relations in porous media incorporating detailed pore structure description. *Transport in Porous Media*, 112(2), 467–487.
- Berg, S., Saxena, N., Shaik, M. & Pradhan, C. (2018) Generation of ground truth images to validate micro-CT image-processing pipelines. *The Leading Edge*, 37(6), 412–420.
- Bradley, D. & Roth, G. (2007) Adaptive thresholding using the integral image. *Journal of Graphics Tools*, 12(2), 13–21.
- Buades, A., Coll, B. & Morel, J.-M. (2005) A non-local algorithm for image denoising. In *2005 IEEE Computer Society Conference on Computer Vision and Pattern Recognition (CVPR'05)*, volume 2. Piscataway, NJ: IEEE, pp. 60–65.
- Chen, H., He, X., Teng, Q., Sheriff, R.E., Feng, J. & Xiong, S. (2020) Super-resolution of real-world rock microcomputed tomography images using cycle-consistent generative adversarial networks. *Physical Review E*, 101(2), 023305.
- Da Wang, Y., Armstrong, R.T. & Mostaghimi, P. (2019) Enhancing resolution of digital rock images with super-resolution convolutional neural networks. *Journal of Petroleum Science and Engineering*, 182, 106261.
- Dong, H., Sun, J., Arif, M., Golsanami, N., Yan, W. & Zhang, Y. (2020) A novel hybrid method for gas hydrate filling modes identification via digital rock. *Marine and Petroleum Geology*, 115, 104255.
- Dvorkin, J., Armbruster, M., Baldwin, C., Fang, Q., Derzhi, N., Gomez, C., Nur, B. & Nur, A. (2008) The future of rock physics: computational methods vs. lab testing. *First Break*, 26(9), 63–68.
- Ebadi, M. (2020) Micro x-ray CT images of two cores (original and filtered). Mendeley Data. Published: 10 June 2020. <https://data.mendeley.com/datasets/tz5zwwgs85v/2>
- Eibenberger, E., Borsdorf, A., Wimmer, A. & Hornegger, J. (2008) Edge-preserving denoising for segmentation in CT-images. In *Bildverarbeitung für die Medizin 2008*. Berlin: Springer, pp. 257–261.
- Gong, G., Zhang, H. & Yao, M. (2015) Speckle noise reduction algorithm with total variation regularization in optical coherence tomography. *Optics Express*, 23(19), 24699–24712.
- Gupta, U. & Ranjan, U. (2022a) Algebraic reconstruction techniques. In *Encyclopedia of mathematical geosciences*. Cham: Springer, pp. 17–24.
- Gupta, U. & Ranjan, U. (2022b) Backprojection tomography. In *Encyclopedia of mathematical geosciences*. Cham: Springer, pp. 1–7.
- Jiang, F., Guo, Y., Tsuji, T., Kato, Y., Shimokawara, M., Esteban, L., Seyyedi, M., Pervukhina, M., Lebedev, M. & Kitamura, R. (2023) Upscaling permeability using multiscale x-ray-CT images with digital rock modeling and deep learning techniques. *Water Resources Research*, 59(3), e2022WR033267.
- Karimpouli, S. & Tahmasebi, P. (2019) Segmentation of digital rock images using deep convolutional autoencoder networks. *Computers & Geosciences*, 126, 142–150.
- Kong, X., Li, K., Yang, Q., Wenyan, L. & Yang, M.-H. (2013) A new image quality metric for image auto-denoising. In *Proceedings of the IEEE International Conference on Computer Vision*. Piscataway, NJ: IEEE, pp. 2888–2895.
- Laine, S., Karras, T., Lehtinen, J. & Aila, T. (2019) High-quality self-supervised deep image denoising. arXiv. <https://doi.org/10.48550/arXiv:1901.10277>
- Landström, A. & Thurley, M.J. (2013) Adaptive morphology using tensor-based elliptical structuring elements. *Pattern Recognition Letters*, 34(12), 1416–1422.
- Lehtinen, J., Munkberg, J., Hasselgren, J., Laine, S., Karras, T., Aittala, M., & Aila, T. (2018) Noise2noise: learning image restoration without clean data. arXiv. <https://doi.org/10.48550/arXiv:1803.04189>
- Liao, Q., You, S., Cui, M., Guo, X., Aljawad, M.S. & Patil, S. (2023) Digital core permeability computation by image processing techniques. *Water*, 15(11), 1995.
- Lindenbaum, M., Fischer, M. & Bruckstein, A. (1994) On Gabor's contribution to image enhancement. *Pattern Recognition*, 27(1), 1–8.
- Liu, M., Ahmad, R., Cai, W. & Mukerji, T. (2023) Hierarchical homogenization with deep-learning-based surrogate model for rapid estimation of effective permeability from digital rocks. *Journal of Geophysical Research: Solid Earth*, 128(2), e2022JB025378.
- Millington, R. & Quirk, J. (1961) Permeability of porous solids. *Transactions of the Faraday Society*, 57, 1200–1207.
- Mohan, E., Rajesh, A., Sunitha, G., Konduru, R.M., Avanija, J. & Ganesh Babu, L. (2021) A deep neural network learning-based speckle noise removal technique for enhancing the quality of synthetic-aperture radar images. *Concurrency and Computation: Practice and Experience*, 33, e6239.
- Niu, Q. & Zhang, C. (2019) Permeability prediction in rocks experiencing mineral precipitation and dissolution: a numerical study. *Water Resources Research*, 55(4), 3107–3121.
- Niu, Y., Mostaghimi, P., Shabaninejad, M., Swietojanski, P. & Armstrong, R.T. (2020) Digital rock segmentation for petrophysical analysis with reduced user bias using convolutional neural networks. *Water Resources Research*, 56(2), e2019WR026597.
- Otsu, N. (1979) A threshold selection method from gray-level histograms. *IEEE Transactions on Systems, Man, and Cybernetics*, 9(1), 62–66.
- Payton, R.L., Chiarella, D. & Kingdon, A. (2022) The upper percolation threshold and porosity–permeability relationship in sandstone reservoirs using digital image analysis. *Scientific Reports*, 12(1), 11311.
- Perona, P. & Malik, J. (1990) Scale-space and edge detection using anisotropic diffusion. *IEEE Transactions on Pattern Analysis and Machine Intelligence*, 12(7), 629–639.
- Reshetova, G., Cheverda, V., Lisitsa, V. & Khachkova, T. (2020) Multi-scale digital rock modelling for reservoir simulation. In *SPE/IATMI Asia Pacific Oil & Gas Conference and Exhibition*. SPE-196561-MS. OnePetro.
- Saxena, N., Hofmann, R., Alpak, F.O., Dietderich, J., Hunter, S. & Day-Stirrat, R.J. (2017) Effect of image segmentation & voxel size on micro-CT computed effective transport & elastic properties. *Marine and Petroleum Geology*, 86, 972–990.
- Saxena, N., Hows, A., Hofmann, R., Alpak, F.O., Dietderich, J., Appel, M., Freeman, J. & De Jong, H. (2019) Rock properties from micro-CT images: digital rock transforms for resolution, pore volume, and field of view. *Advances in Water Resources*, 134, 103419.
- Schepp, L.L., Ahrens, B., Balcewicz, M., Duda, M., Nehler, M., Osorno, M., Uribe, D., Steeb, H., Nigon, B., Stöckert, F., et al., (2020) Digital rock physics and laboratory considerations on a high-porosity volcanic rock: micro-xrct data sets. *Scientific Reports*, 10, 5840.
- Sell, K., Saenger, E.H., Falenty, A., Chaouachi, M., Habberthür, D., Enzmann, F., Kuhs, W.F. & Kersten, M. (2016) On the path to the digital rock physics of gas hydrate-bearing sediments—processing

- of in situ synchrotron-tomography data. *Solid Earth*, 7(4), 12 43–1258.
- Shamsoddini, A., Trinder, J.C., Wagner, W. & Székely, B. (2010) Image texture preservation in speckle noise suppression. Paper presented at the Technical Commission VII Symposium 2010 Abstract Submission System.
- Sheppard, A.P., Sok, R.M. & Averdunk, H. (2004) Techniques for image enhancement and segmentation of tomographic images of porous materials. *Physica A: Statistical Mechanics and Its Applications*, 339(1-2), 145–151.
- Sidorenko, M., Orlov, D., Ebadi, M. & Koroteev, D. (2021) Deep learning in denoising of micro-computed tomography images of rock samples. *Computers & Geosciences*, 151, 104716.
- Smith, S.M. & Brady, J.M. (1997) Susan—a new approach to low level image processing. *International Journal of Computer Vision*, 23(1), 45–78.
- Su, E., Liang, Y., Zou, Q., Niu, F. & Li, L. (2019) Analysis of effects of CO₂ injection on coalbed permeability: implications for coal seam CO₂ sequestration. *Energy & Fuels*, 33(7), 6606–6615.
- Sun, H., Yao, J., Cao, Y.-c., Fan, D.-y. & Zhang, L. (2017) Characterization of gas transport behaviors in shale gas and tight gas reservoirs by digital rock analysis. *International Journal of Heat and Mass Transfer*, 104, 227–239.
- Taud, H., Martinez-Angeles, R., Parrot, J. & Hernandez-Escobedo, L. (2005) Porosity estimation method by x-ray computed tomography. *Journal of Petroleum Science and Engineering*, 47(3), 209–217.
- Tomasi, C. & Manduchi, R. (1998) Bilateral filtering for gray and color images. In *Sixth International Conference on Computer Vision*. Piscataway, NJ: IEEE, pp. 839–846.
- Treece, G. (2016) The bitonic filter: linear filtering in an edge-preserving morphological framework. *IEEE Transactions on Image Processing*, 25(11), 5199–5211.
- Treece, G. (2019) Morphology-based noise reduction: structural variation and thresholding in the bitonic filter. *IEEE Transactions on Image Processing*, 29, 336–350.
- Ulyanov, D., Vedaldi, A. & Lempitsky, V. (2018) Deep image prior. In *Proceedings of the IEEE Conference on Computer Vision and Pattern Recognition*. Piscataway, NJ: IEEE, pp. 9446–9454.
- Verma, R. & Ali, J. (2013) A comparative study of various types of image noise and efficient noise removal techniques. *International Journal of Advanced Research in Computer Science and Software Engineering*, 3(10)
- Verri, I., Della Torre, A., Montenegro, G., Onorati, A., Duca, S., Mora, C., Radaelli, F. & Trombin, G. (2017) Development of a digital rock physics workflow for the analysis of sandstones and tight rocks. *Journal of Petroleum Science and Engineering*, 156, 790–800.
- Wang, X., Ge, L. & Li, X. (2012) Evaluation of filters for Envisat Asar speckle suppression in pasture area. *ISPRS Annals of Photogrammetry, Remote Sensing and Spatial Information Sciences*, 7, 341–346.
- Wang, Z., Bovik, A., Sheikh, H. & Simoncelli, E. (2004) Image quality assessment: from error visibility to structural similarity. *IEEE Transactions on Image Processing*, 13(4), 600–612.
- Wildenschild, D. & Sheppard, A.P. (2013) X-ray imaging and analysis techniques for quantifying pore-scale structure and processes in sub-surface porous medium systems. *Advances in Water Resources*, 51, 217–246.
- Withjack, E. (1988) Computed tomography for rock-property determination and fluid-flow visualization. *SPE Formation Evaluation*, 3(4), 696–704.
- Yaroslavsky, L.P. (2012) *Digital picture processing: an introduction*, Springer Series in Information Sciences, volume 9. Berlin: Springer Science & Business Media.
- Zha, D. (2007) Novel ultrasound images shot noise removal algorithm based on 2-D wavelet decomposition and stable distribution model. In *2007 1st International Conference on Bioinformatics and Biomedical Engineering*. Piscataway, NJ: IEEE, pp. 845–848.
- Zha, D. & Qiu, T. (2006) A new algorithm for shot noise removal in medical ultrasound images based on alpha-stable model. *International Journal of Adaptive Control and Signal Processing*, 20(6), 251–263.
- Zhang, P., Celia, M.A., Bandilla, K.W., Hu, L. & Meegoda, J.N. (2020) A pore-network simulation model of dynamic CO₂ migration in organic-rich shale formations. *Transport in Porous Media*, 133, 479–496.

How to cite this article: Gupta, U., Periyasamy, V., Hofmann, R., Prakash, J. & Yalavarthy, P.K. (2023) Two-step morphology-based denoising and non-local means smoothing improves micro-computed tomography digital rock images. *Geophysical Prospecting*, 1–15.
<https://doi.org/10.1111/1365-2478.13429>